Directing Colloidal Assembly and a Metal-Insulator Transition Using a Quench-Disordered Porous Rod Template

Ryan B. Jadrich and Kenneth S. Schweizer

Phys. Rev. Lett. **113**, 208302 — Published 12 November 2014

DOI: 10.1103/PhysRevLett.113.208302

3nd revision, submitted to Physical Review Letters, October, 2014

Directing Colloidal Assembly and a Metal-Insulator Transition Using a Quench-Disordered Porous Rod Template

Ryan B. Jadrich[1,3] and Kenneth S. Schweizer[1,2,3,*]

Department of Chemistry[1], Department of Materials Science[2], and Frederick Seitz Materials Research Laboratory[3], University of Illinois, Urbana, IL 61801

*kschweiz@illinois.edu

PACS: 64.75.Xc, 81.05.Zx, 72.80.Tm, 64.70.Nd

Abstract

Replica and effective medium theory methods are employed to elucidate how to massively reconfigure a colloidal assembly to achieve globally homogeneous, strongly clustered and percolated equilibrium states of high electrical conductivity at low physical volume fractions. A key idea is to employ a quench disordered, large mesh rigid rod network as a templating internal field. By exploiting bulk phase separation frustration and the tunable competing processes of colloid adsorption on the low dimensional network and fluctuation-driven colloid clustering in the pore spaces, two distinct spatial organizations of greatly enhanced particle contacts can be achieved. As a result, a continuous, but very abrupt, transition from an insulating to metallic-like state can be realized via a small change of either the colloid-template or colloid-colloid attraction strength. The approach is generalizable to more complicated template and/or colloidal architectures.

Colloidal assembly is a promising avenue for the creation of functional materials with superlative thermodynamic, mechanical, optical, electrical and/or structural properties [1-8]. The archetypical approach, equilibrium self-assembly, often utilizes designer particles with specific patchy interactions and/or shape [7-9]. However, their synthesis on the bulk scale is typically limited. As a conceptually distinct alternative, an external or "internal" field can be used to direct assembly [10-14]. For example, polymers can induce effective interactions between particles resulting in diverse structural states such as compact clusters, bridging networks, or full dispersion as a correlated fluid [15,16].

In this Letter, we employ equilibrium statistical mechanical theory to establish a different, largely unexplored, internal field for achieving massively reconfigurable colloidal assembly: a low dimensional, quench disordered, porous and insulating template. Our aim is to discover, and learn how to exploit, the competing physical effects necessary to reversibly trigger an insulator-metal transition at *low* particle concentrations in a mechanically-stable network where macrophase separation is avoided. We demonstrate that a dilute, but interpenetrating, quench disordered rigid rod network composed of meshes or pores large compared to the colloids allows this to be realized via two distinct physical mechanisms.

The first, conceptually simpler mechanism involves the abrupt formation of quasi-one-dimensional colloid multilayers adsorbed on the rod network via a strong enough interfacial (template-colloid) attraction in concert with a judiciously chosen inter-colloid cohesion to induce dense particle packing along the rods. This approach also serves as a reference for the second mechanism based on the template-induced destruction of colloid macrophase separation. This allows the realization of thermodynamically stable, more 3-dimensional, inter-connected networks characterized by high levels of cohesion, clustering, and conductivity that are

inaccessible in the pure bulk fluid phase. Such an approach is qualitatively analogous to using porous media to stabilize molecular fluids such as water in a thermodynamically unstable regime [17], or the use of random external field fluctuations to destroy ferromagnetic ordering per the Quenched Random Field Ising Model (QRFIM) [18,19]. It also suggests a new and more robust route to forming thermoreversible physical gels not complicated by the unavoidable nonequilibrium effects underlying gelation in a spinodal phase separated region of the phase diagram [20-22].

We consider a colloidal fluid (F) of spheres (implicit solvent) immersed in a quenched template (T) of interpenetrating high aspect ratio rigid rods. The minimal description involves 4 structural length scales (rod length, L, rod diameter, d_T, mean network pore radius, $\langle r_P \rangle$, and colloid diameter, d_F), colloidal fluid packing fraction (η_F), and the contact cohesive ($\varepsilon_{F,F}$) and interfacial ($\varepsilon_{T,F}$) attraction energies and their corresponding spatial ranges, $\delta_{T,F} = \delta_{F,F} \equiv \delta$. We are interested in low concentration, long rod networks where $L >> 2\langle r_p \rangle >> d_F >> d_T \geq \delta$; our conclusions are robust to parameters changes in this broad regime [23]. The baseline system employs a rod composed of $n_T = 500$ hard core, tangent, linearly bonded sites of unit diameter ($d_T = 1$), and a dilute colloidal fluid of $\eta_F \equiv \pi \rho_F d_F^3 / 6 = 0.05$. Each template realization is a pure rod fluid equilibrium configuration at a low packing fraction, $\eta_T = 10^{-5}$, corresponding to a $\langle r_P \rangle \cong 113.912 d_T$ [24]. These rods are not literally crosslinked nor forced into close contact; however, since the colloids are very *large* compared to the rod thickness but small compared to the pore diameter, $d_F = 20 d_T$, they can serve as physical crosslinks between the strongly interpenetrating rods to establish a percolated sphere network The site-site cohesive and

interfacial potentials consist of a hard core repulsion plus an exponential attraction: $v_{F,F}(r) = v_{att}(r;\varepsilon_{F,F},d_F,\delta)$, and $v_{T,F}(r) = v_{att}(r;\varepsilon_{T,F},(d_T+d_F)/2,\delta)$, respectively, where beyond contact $v_{att}(r;\varepsilon,d,\delta) = -\varepsilon\exp\left[-(r-d)/\delta\right]$ with $\delta = d_T/2$. Crucially, since $d_F >> d_T$, multiple rod sites interact with an adsorbed sphere; as such, a simple geometry calculation shows that for our interaction potential the *total* rod-sphere attraction strength at contact is $\approx 7\varepsilon_{T,F}$.

To theoretically study this quenched-annealed system we employ the equilibrium Replica Reference Interaction Site Model integral equation approach adapted to treat a macromolecular template [25-30]; all technical details are discussed in the Supplementary Information (SI) [31]. This method predicts both the standard $[g_{T,T}(r), g_{T,F}(r), g_{F,F}(r)]$ and blocking or template-mediated $[\tilde{g}_{F,F}(r)]$ site-site radial distribution functions (SSRDF) where subscripts indicate species. The latter corresponds to a SSRDF between non-interacting fluid clones [26-30]. Metastable states are not predicted as replica symmetry is assumed.

Thermodynamics is characterized by the constant template density dimensionless isothermal compressibility [26]

$$K_{th} \equiv k_B T \rho_F \kappa_T = 1 + 4\pi\rho_F \int_0^\infty dr r^2 \left(g_{F,F}(r) - \tilde{g}_{F,F}(r)\right), \quad (1)$$

which quantifies the long wavelength fluid density fluctuation amplitude that diverges at a spinodal. Local structure is essential for establishing the interparticle contacts required for colloidal percolation and conductivity. It is characterized by a coordination number: the number of colloid sites within the attraction range around either a template site, $\mu = T$, or another colloidal fluid site, $\mu = F$,

$$Z_{\mu,F} = 4\pi\rho_F \int_0^{D_{\mu,F}} dr r^2 g_{\mu,F}(r), \tag{2}$$

where $D_{T,F} \equiv (d_T + d_F)/2 + \delta$ and $D_{F,F} \equiv d_F + \delta$. The hopping electrical conductivity is computed using an accurate effective medium approximation which places a single electron tunneling conductance between all fluid particle pairs, $G(r) \equiv G_0 \exp\left[-2(r - d_F)/\Delta\right]$, where r is the inter-particle separation, G_0 is the contact conductance, and Δ is the short tunneling range (~nm), here set to a representative value of $\Delta = \delta$. From a truncated resistor network Laplacian node pair expansion, a self-consistent equation was derived [43]

$$\int_0^{\infty} dr \frac{4\pi r^2 \rho_F g_{F,F}(r)}{(G^*/G_0)\exp\left[2(r - d_F)/\Delta\right] + 1} = 2, \tag{3}$$

where G^* is the average 2-point network conductance, a useful surrogate for bulk conductivity.

We first consider the simpler "reference" system where interfacial attraction drives an abrupt structural transition. Figure 1A demonstrates the striking variation of K_{th} with $\varepsilon_{T,F}$ at four values of $\varepsilon_{F,F}$ *below* the bulk colloidal fluid spinodal (no template) at $\beta\varepsilon_{F,F} \approx 5$. The wide range in $\varepsilon_{T,F}$ where the fluid is insensitive to the template is abruptly terminated by a cusp-like maximum that grows in amplitude with $\varepsilon_{F,F}$ and/or a precipitous drop associated with onset of a highly incompressible state starting at $\beta\varepsilon_{T,F} \approx 1.18 - 1.21$. The latter signals the formation of an enriched, less compressible layer of particles adsorbed on, or in the vicinity of, the template. The thickness, or the degree of multi-layering, of adsorbed colloids, and their propensity for interparticle contacts, grows with $\varepsilon_{F,F}$; for the hard sphere control case of $\varepsilon_{F,F} = 0$ only monolayer adsorption is possible. We interpret the cusp-like maximum to indicate a state of enhanced particle density fluctuations associated with a maximal bifurcation of colloids into two

populations corresponding to adsorbed on the rods and non-adsorbed in the pores. The adsorption crossover transition becomes softer for larger (smaller) rod density (pore size) [not shown], a natural consequence of obfuscating the distinction between bulk and adsorbed states.

The second structural reconfiguration mechanism utilizes inter-colloid cohesive attractions at high strengths inaccessible in the homogeneous pure colloidal fluid phase. Without the template, increasing fluid cohesion induces a strong monotonic growth of K_{th} and a spinodal divergence at $\beta\varepsilon_{F,F} \approx 5$ as seen by the $\beta\varepsilon_{T,F} = 0$ curve in Figure 1B. In the presence of colloid-template attractions near the above mentioned adsorption crossover at $\beta\varepsilon_{T,F} \approx 1.18 - 1.21$, this growth of K_{th} can be (i) strongly slowed down, (ii) effectively driven to a plateau value, or (iii) decrease just beyond the spinodal, depending on $\beta\varepsilon_{T,F}$ and template density (pore size). The $\beta\varepsilon_{F,F} \geq 5$ regime is a state of thermodynamically stable, avoided spinodal-driven, enhanced clustering that is *inaccessible* to the pure fluid which appears to continue to $\beta\varepsilon_{F,F} \to \infty$. Figure 1B also demonstrates the enhanced efficacy of the template at frustrating macrophase separation as either interfacial attraction or network density is increased [44].

Although entropy plays a quantitative role, the suppression of macrophase separation above a critical value of $\varepsilon_{T,F}$ is fundamentally controlled by when the energy of the templated, partially adsorbed state becomes lower than the phase separated colloidal fluid since both template-colloid and colloid-colloid attractions associated with tight packing along the rod and in the pores can be realized. The critical value of $\beta\varepsilon_{T,F} \approx 1.18 - 1.21$ can be rationalized as the degree of site-level rod-colloid attraction required such that the total colloid-rod cohesion plus colloid-colloid cohesion of particles in close contact along the rod becomes larger than the cohesion realizable in the dense coexisting colloid fluid of a bulk phase separated system [45].

We again emphasize that this phenomenon is qualitatively analogous to the destruction of the ferromagnetic ordering transition beyond a critical random field fluctuation strength [18,19] where spins can achieve a lower free energy by aligning with local random magnetic fields.

We now analyze and contrast the structural and conductivity consequences of the two physically distinct scenarios thermodynamically characterized in Fig.1. Figures 2A and 2B establish the structural signatures of the thermodynamic cusp (adsorption crossover) and steep compressibility reduction at higher $\beta\varepsilon_{F,F}$ seen in Figure 1A. Upon approaching the adsorption crossover from below ($\beta\varepsilon_{T,F} = 1.10$, 1.14), monolayer formation is suggested by the notable first and much weaker higher order coordination shells in $g_{T,F}(r)$, while the local nature of colloid clustering is indicated by the lack of higher order features beyond the trimer correlations in $g_{F,F}(r)$. Far greater particle clustering and qualitatively new structural features abruptly emerge as the interfacial attraction is slightly increased to $\beta\varepsilon_{T,F} = 1.16$ and 1.20 and the cusp in Fig.1A is traversed. Here, $g_{T,F}(r)$ develops a longer range tail indicating diffuse multilayer adsorption on the template, while $g_{F,F}(r)$ develops higher order coordination shells due to particle enrichment proximate to the quenched network.

To better quantify the near contact structural evolution, the coordination numbers $Z_{T,F}$ and $Z_{F,F}$ are plotted in Figures 2C and 2D. Before the adsorption crossover, the magnitude of $Z_{F,F}$ indicates weak to mild clustering in the pores that is essentially insensitive to $\varepsilon_{T,F}$. At the crossover, the intense initial adsorption indicated by the $Z_{T,F}$ results triggers the formation of a dense colloidal multilayer surrounding the template, as manifested by the abrupt upturn in $Z_{F,F}$ which becomes more dramatic as $\varepsilon_{F,F}$ grows (see upper cartoons in Fig.2E). This behavior

stands in qualitative contrast to the entropic drive to spread along the rods upon adsorption as found when there is little or no cohesion (lower cartoons in Fig. 2E).

The above abrupt structural reconfiguration generates a sharp switch between insulating and metallic states (Fig. 2E). At low $\varepsilon_{T,F}$ and $\beta\varepsilon_{F,F} < 5$, the resistance is very high. Beyond $\beta\varepsilon_{T,F} \approx 1.18 - 1.21$, intense template adsorption *and* local particle densification abruptly induce tight particle contacts, thereby establishing facile low resistance pathways for electron transport with a >20 orders of magnitude conductivity increase. The latter is *not* a trivial consequence of adsorption on an interpenetrating rod network, as indicated by the low conductivity for adsorbing hard spheres; rather, tight packing along the rods driven by a sufficiently large $\varepsilon_{F,F} \neq 0$ is essential. The adsorption crossover and metal-insulator transition become sharper by decreasing the rod density (larger pores) thereby providing another tool to tailor the transition (not shown).

The above adsorption-driven clustering mechanism is a promising route to realize massively reconfigurable conductive assemblies. However, given it is associated with a quasi-one-dimensional dense adsorbed colloidal structure, the achievement of high conductivity might be frustrated by structural defects and contact coordination number fluctuations. As we now discuss, the second, even more novel approach (Fig.1B) based on an avoided spinodal transition results in a qualitatively distinct percolated colloidal network of an effectively higher dimensionality and microphase-separation-like character, and should be a more robust alternative in practice. Figures 3A and 3B show the large real space structural transformations that emerge upon approaching the bulk spinodal attraction strength from below. Both $g_{T,F}(r)$ and $g_{F,F}(r)$ indicate the onset of strong clustering via the development of a crisp second coordination shell and longer range tail. For $\beta\varepsilon_{F,F} \geq 5$, $g_{F,F}(r)$ rapidly increases locally and new higher (beyond

second) order coordination shells emerge. In qualitative contrast to the first mechanism, $g_{T,F}(r)$ *decreases* above $\beta\varepsilon_{F,F} \approx 5$. These structural changes collectively suggest a transition to a state with both significant network adsorption *and* inter-pore clustering via "bridging connections" between the rod-templated particles, as depicted by the cartoons in Fig. 3E. Additional support for the latter interpretation is given in the SI [31] where we show the emergence for $\beta\varepsilon_{F,F} > 5$ of a low wavevector, microphase-separation-like peak or feature in the colloid-colloid collective structure factor on the large mesh length scale dictated by the template network.

Avoided spinodal induced clustering is effectively contrasted to its alternative adsorption-driven analog by examining the coordination numbers in Figs. 3C and 3D. Unlike in the adsorption scenario, $Z_{T,F}$ is highly *non-monotonic* with a maximum at the avoided spinodal. Initial adsorption occurs for the reasons discussed in the context of Fig. 2D. But beyond the avoided spinodal, the long range density fluctuations and greater clustering attainable in the bulk drive some adsorbed colloids back into the pores. The top cartoons in Fig. 3E suggest a highly inter-connected, more 3-dimensional clustered state, an inference further supported by the marked growth in $Z_{F,F}$ beyond $\beta\varepsilon_{F,F} \approx 5$. This behavior becomes more dramatic as $\beta\varepsilon_{T,F}$ decreases, albeit remains above the critical value required to suppress macrophase separation.

Figure 3E shows that the second structural reconfiguration mechanism results in huge conductivity enhancement. With a small increase of colloid cohesion beyond $\beta\varepsilon_{F,F} \approx 5$ a sharp structural reorganization connects *thermodynamically stable* metal and insulating states with conductivities differing by > 20 orders of magnitude. This transition is tunable, and is more abrupt for a weaker $\varepsilon_{T,F}$. Decreasing rod density exaggerates the amplitude and sharpness of the metal-insulator transition by destabilizing the fluid against macrophase separation [46].

Besides providing a route to achieve a sharp metal-insulator transition, the avoided spinodal phenomenon elucidated here has broader relevance. For example, it suggests a novel way to achieve *equilibrium*, globally homogeneous, thermoreversible particle gelation that avoids the nonequilibrium complications of kinetic gelation in a 2-phase spinodal region [20-22]. This fundamental problem has been recently discussed based on simulations of patchy particle models of limited valence where the coordination number is geometrically restricted [20,21]. Such a strategy does lead to a large reduction of the critical point packing fraction and shrinkage of the phase separated regime towards low density, with reversible gelation at volume fractions as low as ≈ 0.2 being realized [20,21]. We believe our approach significantly improves on this by completely eradicating the two phase region thereby enabling reversible gelation into a 3-dimensionally connected structure in very dilute rod networks at all particle densities that percolate. Moreover, the ability to tune the amplitude of density fluctuations via $\varepsilon_{T,F}$ provides a way to interpolate between spinodal-like and reversible homogeneous gelation, and gels produced via a temperature (effective cohesion strength) quench will age towards a well-defined equilibrium endpoint of high and stable connectivity.

Finally, we briefly comment on how the systems theoretically analyzed in this paper might be realized experimentally. Well-studied, highly tunable biological networks of long, thin, rod-like polymers (e.g., fibrin, microtubules) can furnish the large pores (up to 10 microns) required to achieve the desired $2\langle r_p \rangle >> d_F$ inequality [47]. Colloids of various chemistry can be stabilized via Coulomb repulsion or repulsive (neutral or polyelectrolyte) brush layers to achieve $\varepsilon_{F,F} \approx 0$. By varying solution pH, the biopolymer network charge can manipulated to attract oppositely charged colloids [48], and salt concentration can control the range of $\varepsilon_{T,F}$. Inter-colloid cohesion ($\varepsilon_{F,F}$) of van der Waals attraction origin could be potentially controlled by

employing a temperature-induced collapse or expansion of a thermoreversible brush [49]. Of course, the simultaneous control of $\varepsilon_{T,F}$ and $\varepsilon_{F,F}$ will be subtle in practice, and limitations in synthesizing monodisperse colloids and/or rods will soften structural and conductivity transitions. However, the use of biopolymers and model colloids can likely minimize the latter.

In summary, we have used theory to discover, and formulate design rules for, two distinct approaches for the creation of massively reconfigurable and electrically conductive, but physically dilute and mechanically stable, colloidal assemblies based on a large mesh quenched rod network. Although our methods must incur quantitative errors, prior studies using RISM and replica methods [25-30] suggest they are likely modest, and certainly the basic phenomena of sharp adsorption and destruction of bulk demixing are expected to be captured qualitatively correctly by the theory; future simulations are needed to check the quantitative accuracy. Importantly for experiment, the proposed mechanisms are qualitatively robust [23] to variation of the system-specific variables within the broad inequality range of $L \gg 2\langle r_p \rangle \gg d_F \gg d_T \geq \delta$. The approach can treat bendable rods (e.g., nanotubes, biopolymers), nonspherical particles, and Janus colloids. It also sets the stage (equilibrium endpoints) for developing new theories for the nonequilibrium dynamics of switching between metallic and insulating configurations, and the formation of globally homogeneous physical gels in adsorbing networks.

Acknowledgments: We thank Paul Braun, Randy Ewoldt, Martin Gruebele and Zachary Dell for valuable discussions. RBJ thanks Beth Anne Lindquist for helpful conversations and a constructive critique of the manuscript. This work was supported by DOE-BES under Grant No. DE-FG02-07ER46471 administered through the Frederick Seitz Materials Research Laboratory.

References:

[1] V. J. Anderson and H. N. W. Lekkerkerker, Nature **416**, 811-815 (2002).

[2] J. Mewis, N. J. Wagner, Colloidal Suspension Rheology (Cambridge University Press, New York, 2012).

[3] V. Kobelev and K. S. Schweizer, Phys. Rev. E **71**, 021401(2005).

[4] K. L. Kelly , E. Coronado , L. L. Zhao , and G. C. Schatz, J. Phys. Chem. B **107**, 668-677 (2003).

[5] S. Nam, H. W. Cho, S. Lim, D. Kim, H. Kim, and B. J. Sung, ACS Nano. **7**, 851–856 (2013).

[6] B. Y. Ahn, E. B. Duoss, M. J. Motala, X. Guo, S. Park, Y. Xiong, J. Yoon, R. G. Nuzzo, J. A. Rogers and J. A. Lewis, Science **20**, 1590 (2009).

[7] Q. Chen, S. C. Bae, and S. Granick, Nature **469**, 381 (2011); X. Mao, Q. Chen, S. Granick, Nature Materials **12**, 217 (2013).

[8] A. A. Shah, B. A. Schultz, K. L. Kohlstedt, S. C. Glotzer and M. J. Solomon, Langmuir **29**, 15 4688-4696 (2013).

[9] G-R. Yi, D. J Pine and S. Sacanna, J. Phys.-Cond. Mat. **25**, 193101 (2013).

[10] J. Yan, M. Bloom, S. C. Bae, E. Luijten, and S. Granick, Nature **491**, 578 (2012).

[11] J. W. Swan, J. L. Bauer, Y. Liu and E. M. Furst, Soft Matter, **10**, 1102–1109 (2014).

[12] E. M. Furst, Soft Matter, **9**, 9039–9045 (2013); E. M. Furst, Proc. Nat. Acad. Sci. **108**, 20853–20854 (2011).

[13] A. A. Shah, H. Kang, K. L. Kohlstedt, K. H. Ahn, S. C. Glotzer, C. W. Monroe and M. J. Solomon, Small **8**, 1551–1562 (2012).

[14] Y. Kim, A. A. Shah and M. J. Solomon, Nature Communications **5**, 3676 (2013).

[15] K. I. Winey and R. A. Vaia, MRS Bull. **32**, 314 (2007).

[16] L. M. Hall, A. Jayaraman, and K. S. Schweizer, Current Opinion in Solid State and Materials Science **14**, 38-48 (2010).

[17] K-H. Liu, Y. Zhang, J-J. Lee, C-C. Chen, Y-Q. Yeh, S-H. Chen, C-Y. Mou, J. Chem. Phys. **139**, 064502 (2013).

[18] A. Aharony, Phys. Rev. B **18**, 3318 (1978); M. Mezard and R. Monasson, Phys. Rev. B **50**, 7199 (1994).

[19] N. G. Fytas and V. Martín-Mayor, Phys. Rev. Lett. **110**, 227201 (2013); F. Krzakala, F. Ricci-Tersenghi, and L. Zdeborová, Phys. Rev. Lett. **104**, 207208 (2010).

[20] A. J. Moreno, S.V. Buldyrev, E. La Nave, I. Saika-Voivod, F. Sciortino, P. Tartaglia, and E. Zaccarelli, Phys. Rev. Lett. **95**, 157802 (2005); E. Zaccarelli, S.V. Buldyrev, E. La Nave, A. J. Moreno, I. Saika-Voivod, F. Sciortino and P. Tartaglia, Phys. Rev. Lett. **94**, 218301 (2005).

[21] F. Sciortino, S. V. Buldyrev, C. De Michele, G. Foffi, N. Ghofraniha, E. La Nave, A. Moreno, S. Mossa, I. Saika-Voivod, P. Tartaglia, E. Zaccarelli, Computer Physics Communications **169**, 166–171 (2005).

[22] P. J. Lu, E. Zaccarelli, F. Ciulla, A. B. Schofield, F. Sciortino and D. A. Weitz, Nature **453**, 499-503 (2008); W. C. K. Poon, A. D. Pirie and P. N. Pusey, Faraday Discuss., **101**, 65-76 (1995).

[23] R. Jadrich and K. S. Schweizer, unpublished calculations.

[24] A. G. Ogston, B. N. Preston and J. D. Wells, Proc. R. Soc. Ser. A **333**, 297 (1973).

[25] J. P. Hansen and J. R. McDonald, Theory of Simple Liquids, 2nd ed. (Academic, London, 1986).

[26] M. L. Rosinberg, G. Tarjus and G. Stell, J. Chem. Phys. **100**, 5172 (1994); J. A. Given and G. Stell, Physica A. **209**, 495-510 (1994).

[27] A. Meroni, D. Levesque and J. J. Weis, J. Chem. Phys. **105**, 1101 (1996).

[28] A. Kovalenko and F. Hirata, J. Chem. Phys. **115**, 8620 (2001).

[29] L. Sarkisov and P. R. Van Tassel, J. Phys. Chem. C **111**, 15726-15735 (2007).

[30] A. Yethiraj, J. Chem. Phys. **116**, 5910 (2002); B. J. Sung and A. Yethiraj, J. Chem. Phys. **123**, 074909 (2005).

[31] See Supplemental Material [url], which includes Refs. [25-28,30,32-42].

[32] V. Dotsenko, Introduction to the Replica Theory of Disordered Statistical Systems (Cambridge University Press, New York, 2001) and references therein.

[33] M. Mezard, G. Parisi, and M.A. Virasoro: Spin Glass Theory and Beyond (World Scientific, Singapore, 1987) and references therein.

[34] M. L. Rosinberg, G. Tarjus and G. Stell, J. Chem. Phys. **100**, 5172 (1994).

[35] L. Sarkisov and P. R. Van Tassel, J. Chem. Phys. **123**, 164706 (2005).

[36] D. Chandler and H. C. Andersen, J. Chem. Phys. **57**, 1930 (1972).

[37] D. Chandler in Studies in Statistical Mechanics, edited by E. W. Montroll and J. L. Lebowitz (North Holland, Amsterdam, 1982).

[38] D. M. Richardson and D. Chandler, J. Chem. Phys. **80**, 4464 (1984).

[39] P. T. Cummings and G. Stell, Mol. Phys. **46**, 383426 (1982).

[40] K. S. Schweizer and J. G. Curro, Adv. Chem. Phys., **98**, 1 (1997).

[41] G. A. Martynov and G. N. Sarkisov, Mol. Phys. **49**, 1495-1504 (1983).

[42] A. C. Hindmarsh, P. N. Brown, K. E. Grant, S. L. Lee, R. Serban, D. E. Shumaker, and C. S. Woodward, ACM Transactions on Mathematical Software **31**, 363-396 (2005).

[43] C. Grimaldi, EPL **96**, 36004 (2011); G. Ambrosetti, I. Balberg, and C. Grimaldi, Phys. Rev. B **82**, 134201 (2010).

[44] Numerically, the critical interfacial attraction strength needed to destroy bulk phase separation cannot be determined quantitatively, but we do find that $1/K_{th}$ for $\varepsilon_{F,F}$ proximate to the bulk spinodal value increases strongly with $\varepsilon_{T,F}$ in a manner highly suggestive of a *finite* critical temperature (or $\varepsilon_{T,F}$).

[45] If colloids undergo bulk demixing, the coexisting dense fluid cohesive energy per particle is $\approx 5k_BT$ times the number of contact neighbors; avoiding double counting, this is $\approx 15-25\,k_BT$. The competing process of adsorption ($\approx 7\,k_BT$ per particle) and inter-colloid attraction in the adsorbed state ($\approx 15\,k_BT$ for three neighbors) yields a comparable level of stabilization of $\approx 22\,k_BT$.

[46] Notable gains in conductivity are realizable in the template-free fluid but would require an experimentally impractical ultrafine control of the interactions to position the system arbitrarily close, but not beyond, the bulk spinodal. Such a system would also lack mechanical integrity.

[47] M. Molteni, D. Magatti, B. Cardinali, M. Rocco, and F. Ferri, Biophys. J., **104**, 1160-1169 (2013); D. Magatti, M. Molteni, B. Cardinali, M. Rocco, and F. Ferri, Biophys. J., **104**, 1151-1159 (2013).

[48] E. Spruijt, H. E. Bakker, T. E. Kodger, J. Sprakel, M. A. Cohen Stuarta and J. van der Guchta, Soft Matter, **7**, 8281-8290 (2011).

[49] A. P. R. Eberle, R. Castañeda-Priego, J. M. Kim, and N. J. Wagner, Langmuir **28**, 1866−1878 (2012); A. P. R. Eberle, N. J. Wagner, and R. Castañeda-Priego Phys. Rev. Lett. **106**, 105704 (2011).

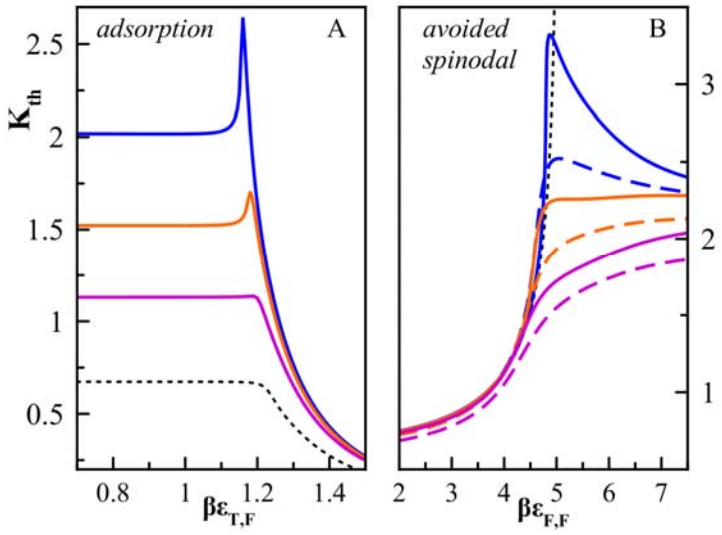

Figure 1. Frame A: from bottom to top the dimensionless compressibility as a function of $\beta\varepsilon_{T,F}$ for $\beta\varepsilon_{F,F}=0$ (dashed black), 4 (magenta), 4.5 (orange) and 4.75 (blue), respectively, at $\eta_T=0.00001$. Frame B: Corresponding quantity based on varying $\beta\varepsilon_{F,F}$. Solid and long dashed curves correspond to $\eta_T=0.00001$ and $\eta_T=0.00008$ (mean pore radius of $\approx 40d_T$) respectively, and bottom to top are for fixed $\beta\varepsilon_{T,F}=1.2$ (magenta), 1.175 (orange) and 1.15 (blue) respectively. The thin dashed black curve corresponds to $\beta\varepsilon_{T,F}=0$.

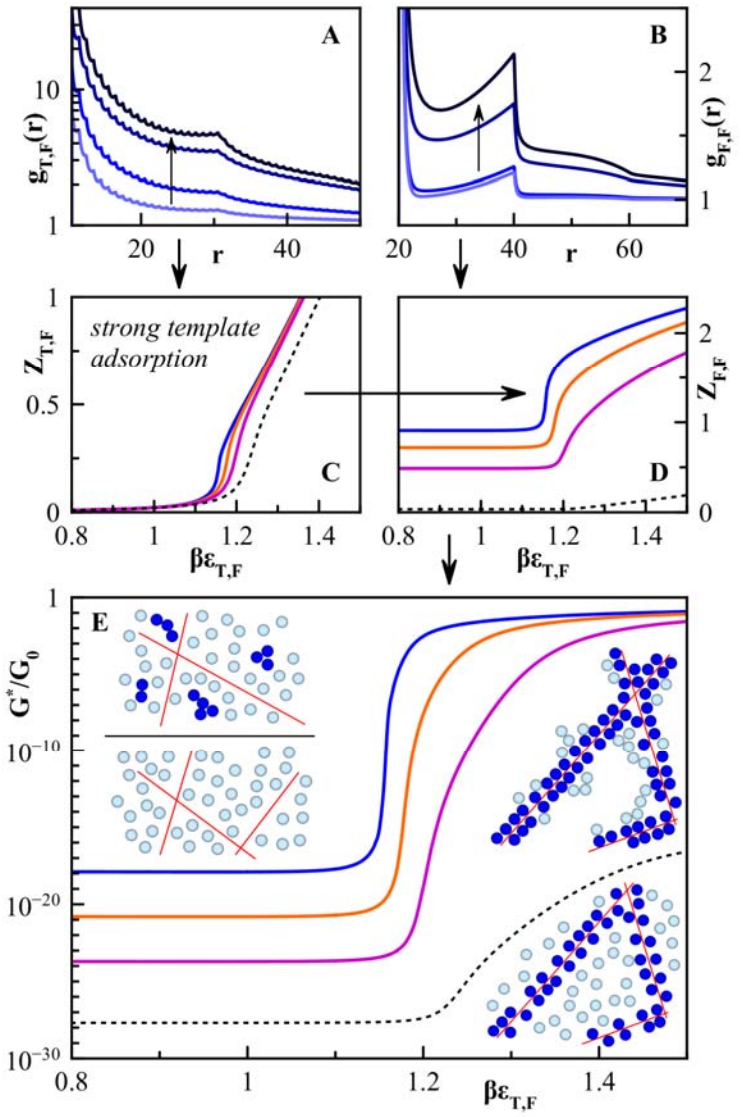

Figure 2. Frames A and B: radial distribution functions at $\beta\varepsilon_{F,F} = 4.75$ for $\beta\varepsilon_{T,F} = 1.10$, 1.14, 1.16 and 1.20 in order of increasing darkness and arrows. Frames C and D: from left to right the coordination number for $\beta\varepsilon_{F,F} = 4.75$ (blue), 4.5 (orange), 4 (magenta) and zero (dashed black). Frame E: from left to right the dimensionless conductivity for $\beta\varepsilon_{F,F} = 4.75$ (blue), 4.5 (orange), 4 (magenta), and zero (dashed black).

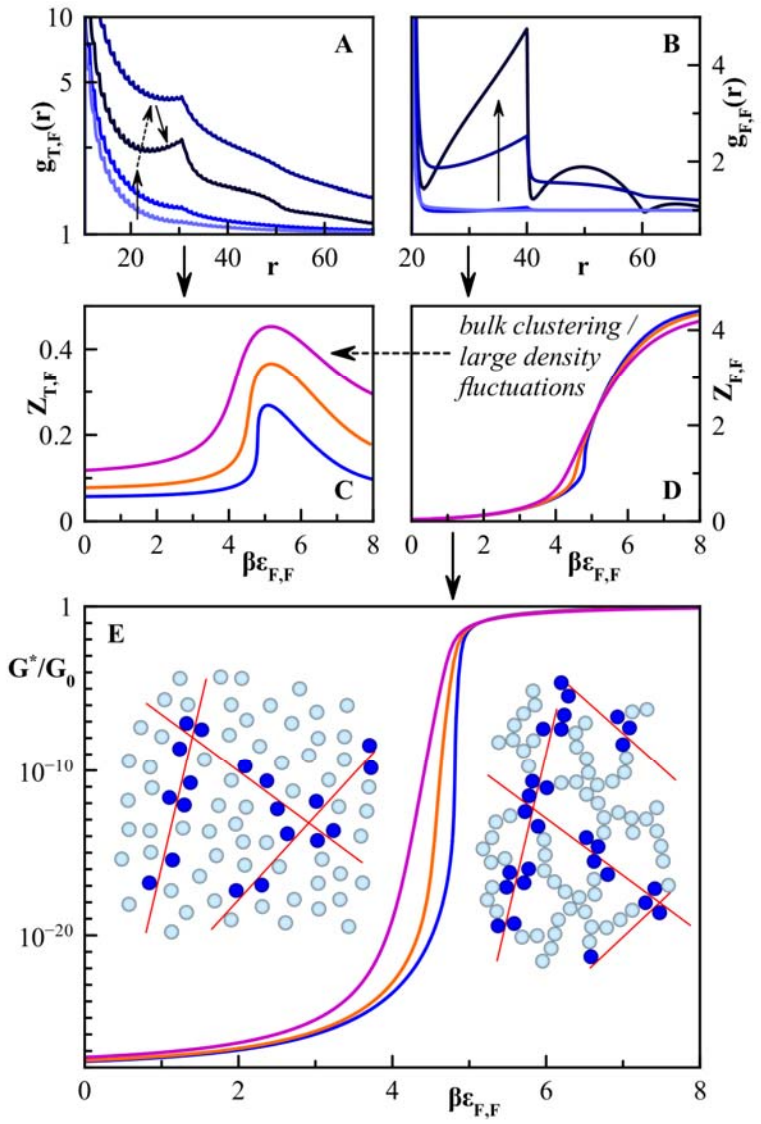

Figure 3. Frames A and B: radial distribution functions at $\beta\varepsilon_{T,F}=1.15$ for $\beta\varepsilon_{F,F}=2$, 4, 5 and 7 in order of increasing darkness and arrows. Frame C {D}: from top to bottom {bottom to top on right most side} the coordination number for $\beta\varepsilon_{T,F}=1.2$ (magenta), 1.175 (orange), and 1.15 (blue). Frame E: From left to right the dimensionless conductivity for $\beta\varepsilon_{T,F}=1.2$ (magenta), 1.175 (orange), and 1.15 (blue).